Supplementary Information

High-order Pair-reduced Neural Network Architecture for Global Potential Energy Surface Exploration Across the Periodic Table

Zheng-Xin Yang[#1], Zhen-Xiong Wang[#1], Xin-Tian Xie[#1], Dong-Xiao Chen, Zi-Xing, Guo, Jia-Jie Du, Qian-Yu Liu, Cheng Shang[1]*, Zhi-Pan Liu[1,2]*

[1]State Key Laboratory of Porous Materials for Separation and Conversion, Collaborative Innovation Center of Chemistry for Energy Material, Shanghai Key Laboratory of Molecular Catalysis and Innovative Materials, Key Laboratory of Computational Physical Science, Department of Chemistry, Fudan University, Shanghai 200433, China

[2]State Key Laboratory of Metal Organic Chemistry, Shanghai Institute of Organic Chemistry, Chinese Academy of Sciences, Shanghai 200032, China

[#]authors contribute equally to this work.

[*]email: cshang@fudan.edu.cn; zpliu@fudan.edu.cn

Contents

Supplementary Tables

Supplementary Table S1: HPNN Performance with Varying Spherical Harmonic degrees on TiO_2 Dataset. Performance of HPNN models with different spherical function degrees(*l*) on the global Ti-O dataset, including Root Mean Square Error (RMSE) for energy (E-RMSE, meV) and force (F-RMSE, eV/Å), and training time(GPU seconds). Best results in bold.

HPNN with different angular interaction schemes [$]	No. Params	Train Time (sec.)	Train Loss		Test Loss	
			E-RMSE (meV)	F-RMSE (eV/Å)	E-RMSE (meV)	F-RMSE (eV/Å)
[0,1], [0,1], [0,1]	1.22M	**7.1**	6.60	0.115	9.85	0.167
[0,1], [0,2], [0,4]	1.22M	9.2	5.96	0.097	7.52	0.134
[0,4], [0,2], [0,1]	1.22M	9.3	5.71	0.096	**6.34**	0.128
[0,1,2], [0,1,2], [0,1,2]	1.51M	10.0	4.66	0.086	7.31	0.135
[0,1,4], [0,1,2], [0,1,1]	1.51M	11.2	4.86	0.086	7.57	0.126
[0,1,6], [0,1,4], [0,1,2]*	1.51M	15.4	**4.44**	**0.080**	6.41	**0.125**
[0,6], [0,4], [0,2], [0,1]	1.55M	14.8	4.47	0.084	7.56	**0.125**

[$]: The HP layer sequence follows from left to right; the digital in [ ] indicates the degree *l*.

*: the one utilized in the final HPNN models throughout the work.

Supplementary Table S2: Inference Time Comparison on NVIDIA RTX 4090 GPU. Inference time comparison (ms) of PaiNN[1], MACE[2], and HPNN on a 4090 GPU for systems with varying numbers of atoms.

Number of Atoms	PaiNN Time (ms)	MACE Time (ms)	HPNN Time (ms)
96	11.916	53.601	13.665
480	39.700	145.510	23.022
960	50.176	274.750	32.475
1920	72.155	530.460	49.132
3840	113.403	-	91.381
5760	160.762	-	133.584
8160	225.247	-	201.558

Supplementary Table S3: Single- and Multi-GPU HPNN Inference Times. Comparison of single-GPU and multi-GPU HPNN inference times (ms) on a 4090 GPU, including neighbor search and energy/force evaluation.

Number of Atoms	Single-GPU Total Time (ms)	Single-GPU Neighbor Search (ms)	Single-GPU Energy/Force (ms)	Multi-GPU Total Time (ms)	Multi-GPU Neighbor Search (ms)	Multi-GPU Energy/Force (ms)
96	13.665	0.663	13.002	64.339	2.92	61.419
960	32.475	3.675	28.8	68.747	3.33	65.417
1920	49.132	9.691	39.441	70.124	3.13	66.994
3840	91.381	15.853	75.528	76.145	3.71	72.435
5760	133.584	22.856	110.728	89.214	3.96	85.254
8160	201.558	34.847	166.711	97.279	4.33	92.949
14400	-	-	-	126.282	5.36	120.922
19200	-	-	-	154.953	5.43	149.523

Supplementary Table S4: Detailed results for Performance of GG-NN Potential in Predicting CO activation in Fischer-Tropsch Synthesis. Gibbs Free Energies (eV) of Initial, Transition, and Final States on Fe_5C_2 (510) Surface in Fischer-Tropsch Synthesis, Calculated by DFT, GG-NN, and LASP CPU Potentials (The reaction conditions are set at T = 523 K, P = 2.5 MPa, H_2/CO = 2 for computing the Gibbs free energy[3].)

	IS(eV)	TS(eV)	FS(eV)
	C_{Cv}+H→CH_{Cv}		
Molecular structure	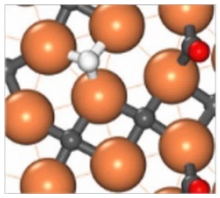	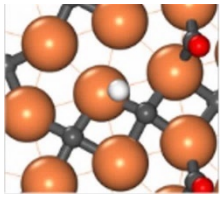	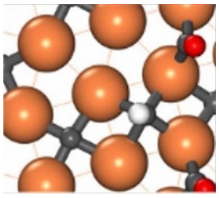
G(DFT)	0.00	0.85	0.22
G(GG-NN potential)	0.00	0.89	0.26
G (LASP CPU potential)	0.00	1.00	0.26
	CH_{Cv}→CH+C_{Cv}		
Molecular structure	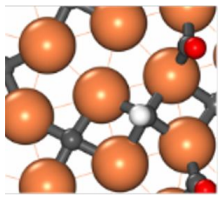	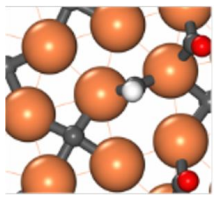	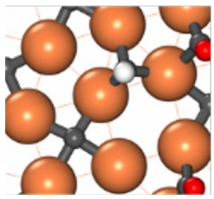
G(DFT)	0.22	0.97	0.72
G(GG-NN potential)	0.26	0.96	0.64
G (LASP CPU potential)	0.26	1.00	0.51
	CH+CO_{Cv}→CH+C_{Cv}+O		
Molecular structure	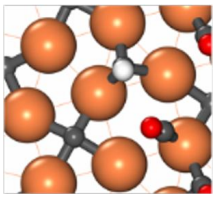	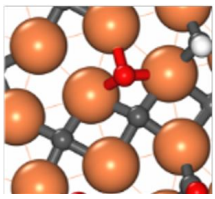	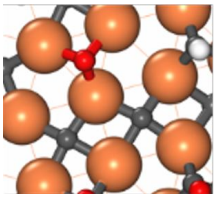
G(DFT)	-0.01	1.15	-0.14
G(GG-NN potential)	-0.06	1.22	-0.20
G (LASP CPU potential)	-0.10	1.12	-0.18
	CH+C_{Cv}+O+H→CCH_{Cv}+O+H		
Molecular structure	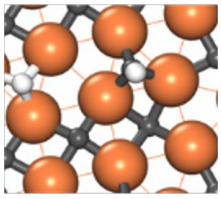	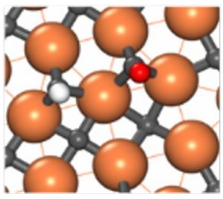	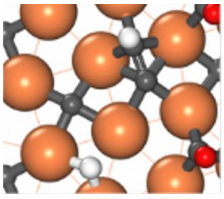
G(DFT)	-0.38	0.10	-0.62
G(GG-NN potential)	-0.44	0.10	-0.60
G (LASP CPU potential)	-0.48	0.04	-0.52

Supplementary Table S5: Structure Information for Ti–O Dataset. Structure information for the Ti–O dataset (27,278 structures) used in neural network training, including chemical formula, number of atoms (N_{atoms}), structure type (cluster, bulk, layer), and total number (N_{total}).

Chemical Formula	N_{atoms}	cluster	layer	bulk	N_{total}
Ti_8	8	0	11	95	106
Ti_{13}	13	0	7	5	12
Ti_{16}	16	1011	2	3468	4481
Ti_{21}	21	0	3	1276	1279
Ti_{32}	32	0	5	304	309
O_1-Ti_{12}	13	0	1437	0	1437
O_2-Ti_8	10	0	92	294	386
O_2-Ti_{10}	12	0	784	0	784
O_3-Ti_{18}	21	0	133	0	133
O_4	4	0	84	0	84
O_4-Ti_4	8	0	163	551	714
O_4-Ti_8	12	0	88	326	414
O_4-Ti_{22}	26	0	8	26	34
O_5-Ti_{27}	32	0	0	29	29
O_6-Ti_4	10	0	0	38	38
O_6-Ti_8	14	0	95	388	483
O_6-Ti_{15}	21	0	111	0	111
O_6-Ti_{18}	24	0	7	50	57
O_8-Ti_4	12	1892	173	10320	12385
O_8-Ti_8	16	0	87	327	414
O_8-Ti_{15}	23	0	21	39	60
O_{10}-Ti_8	18	0	119	399	518
O_{10}-Ti_{22}	32	0	0	29	29
O_{11}	11	0	442	138	580
O_{12}-Ti_8	20	0	0	338	338
O_{13}-Ti_6	19	0	133	433	566
O_{13}-Ti_7	20	0	39	19	58
O_{14}-Ti_7	21	0	0	1	1
O_{14}-Ti_8	22	0	0	179	179
O_{15}-Ti_9	24	0	2	263	265
O_{16}-Ti_8	24	0	116	497	613
O_{18}-Ti_8	26	0	0	2	2
O_{18}-Ti_{12}	30	0	310	16	326
O_{120}-Ti_{59}	179	0	1	8	9
O_{120}-Ti_{60}	180	0	1	0	1
O_{126}-Ti_{63}	189	0	0	15	15
O_{126}-Ti_{64}	190	0	0	12	12
O_{127}-Ti_{63}	190	0	0	1	1
O_{127}-Ti_{64}	191	0	0	1	1
O_{128}-Ti_{63}	191	0	0	3	3

O_{128}-Ti_{64}	192	0	0	9	9
O_{239}-Ti_{119}	358	0	1	0	1
O_{240}-Ti_{120}	360	0	1	0	1
total	--	2903	4476	19899	27278

Supplementary Table S6: Performance and Architecture of Models on Ti–O Dataset. Performance and architectural details of HPNN, PaiNN[1], Nequip[4], Allegro[5], and MACE[2] models on the Ti-O global dataset, including node dimension N_n, pair dimension N_p, scalar node feature dimension N_{sca}, vector components node feature dimension N_{vec}, Maximum Angular Momentum (l_{max}), parameters, training time (GPU seconds), train/test energy RMSE(meV), and force RMSE(eV/Å).

Model	N_n		N_p	l_{max}	No. Params	Train Time (GPU sec.)	Train E-RMSE (meV)	Train F-RMSE (eV/Å)	Test E-RMSE (meV)	Test F-RMSE (eV/Å)
	N_{sca}	N_{vec}								
HPNN	256	0	128	6	1.55M	15.40	4.44	0.080	6.41	0.125
PaiNN	196	196*3	196	1	1.40M	18.70	7.31	0.051	13.00	0.187
Nequip	64	64*8	64	2	1.44M	203.00	6.27	0.094	15.50	0.179
Allegro	64	64*8	64	2	1.30M	121.50	3.84	0.047	14.60	0.160
MACE	128	128*3	128	2	1.47M	111.90	6.40	0.051	10.30	0.131

Supplementary Table S7: Barrier Prediction Errors for Organic Reactions on C–H–O Dataset. Barrier prediction errors for 24 organic reactions using HPNN, PaiNN, MACE, and GG-NN on C-H-O Dataset (eV)

Molecular structure		DFT (eV)	HPNN (eV)	PaiNN (eV)	MACE (eV)	GG-NN (eV)
Claisen rearrangement						
IS	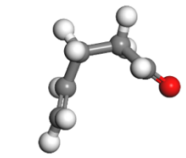	-80.224	-80.232	-80.232	-80.219	-80.261
FS	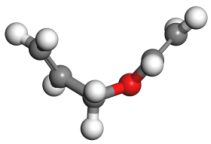	-78.547	-78.545	-78.548	-78.549	-78.553
TS	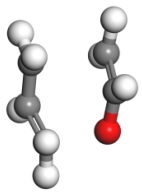	-79.444	-79.449	-79.447	-79.444	-79.427
D-glucose→Glucopyranose						

IS	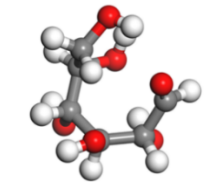	-137.121	-137.109	-137.124	-137.104	-137.152
FS	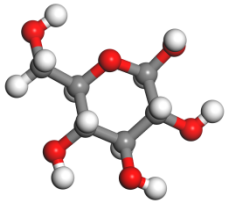	-137.519	-137.523	-137.526	-137.539	-137.605
TS	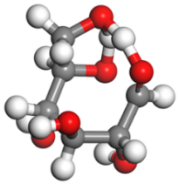	-136.433	-136.445	-136.446	-136.456	-136.543
Glucofuranose→Glucopyranose						
IS	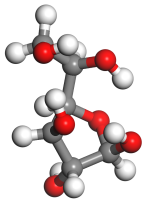	-137.992	-137.998	-138.006	-137.945	-138.010
FS	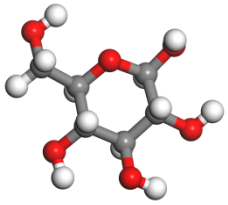	-137.879	-137.874	-137.874	-137.880	-137.911
TS	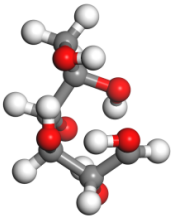	-137.336	-137.326	-137.342	-137.349	-137.329
Glucopyranose→Glucoseptanose						
IS	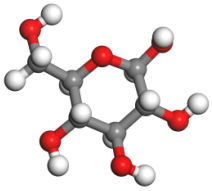	-137.668	-137.635	-137.663	-137.618	-137.643
FS	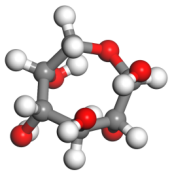	-137.720	-137.720	-137.714	-137.726	-137.768

TS	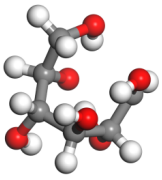	-137.645	-137.632	-137.656	-137.657	-137.678
2,5-Anhydro-D-mannose→Glucopyranose						
IS	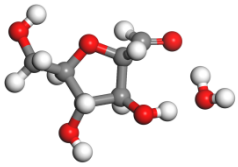	-137.668	-137.635	-137.663	-137.618	-137.643
FS	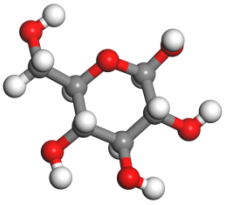	-137.720	-137.720	-137.714	-137.726	-137.768
TS	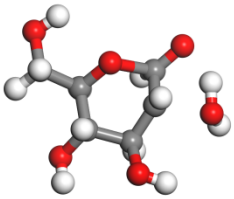	-137.645	-137.632	-137.656	-137.657	-137.678
$H_3CCHO \rightarrow H_2CCHOH$						
IS	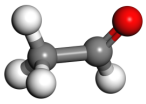	-39.084	-39.089	-39.089	-39.090	-39.126
FS	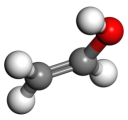	-38.733	-38.731	-38.732	-38.743	-38.739
TS	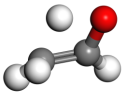	-36.480	-36.478	-36.479	-36.458	-36.407
$H_2CO \rightarrow H_2+CO$						
IS	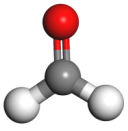	-22.134	-22.133	-22.134	-22.132	-22.159
FS	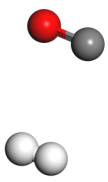	-21.531	-21.530	-21.529	-21.526	-21.561

TS	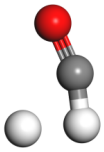	-18.711	-18.717	-18.717	-18.706	-18.661
			HCCH→CCH_2			
IS	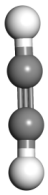	-22.942	-22.940	-22.943	-22.946	-22.948
FS	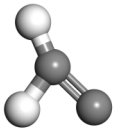	-20.972	-20.972	-20.973	-20.974	-20.955
TS	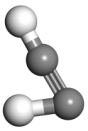	-20.994	-21.000	-20.992	-20.989	-21.005
			Parent Diels-Alder			
IS	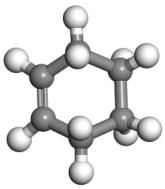	-90.569	-90.575	-90.579	-90.608	-90.588
FS	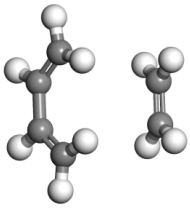	-88.766	-88.771	-88.768	-88.768	-88.788
TS	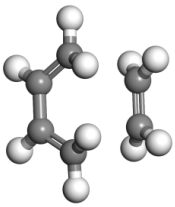	-88.245	-88.262	-88.262	-88.231	-88.235
			Acrolein rotation			
IS	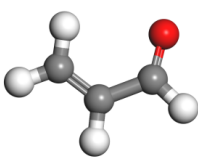	-47.245	-47.257	-47.246	-47.269	-47.277

FS	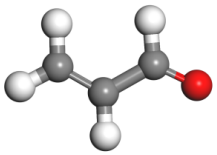	-47.357	-47.365	-47.362	-47.334	-47.373
TS	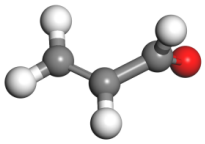	-46.976	-46.986	-46.985	-46.999	-46.964
	Glucopyranose→Levoglucosan					
IS	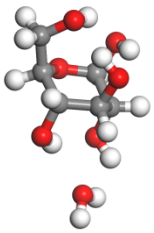	-137.878	-137.857	-137.892	-137.867	-137.900
FS	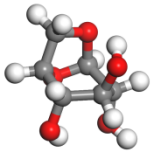	-137.872	-137.880	-137.898	-137.892	-137.975
TS	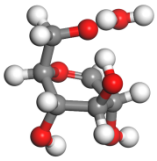	-136.218	-136.206	-136.191	-136.177	-136.215
	Butadiene rotation					
IS	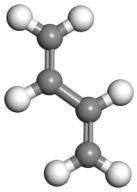	-56.998	-57.009	-56.978	-56.976	-56.979
FS	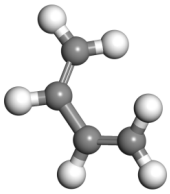	-56.843	-56.826	-56.803	-56.812	-56.784
TS	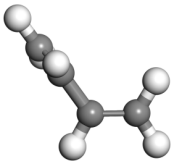	-56.676	-56.662	-56.696	-56.698	-56.597

Supplementary Figures

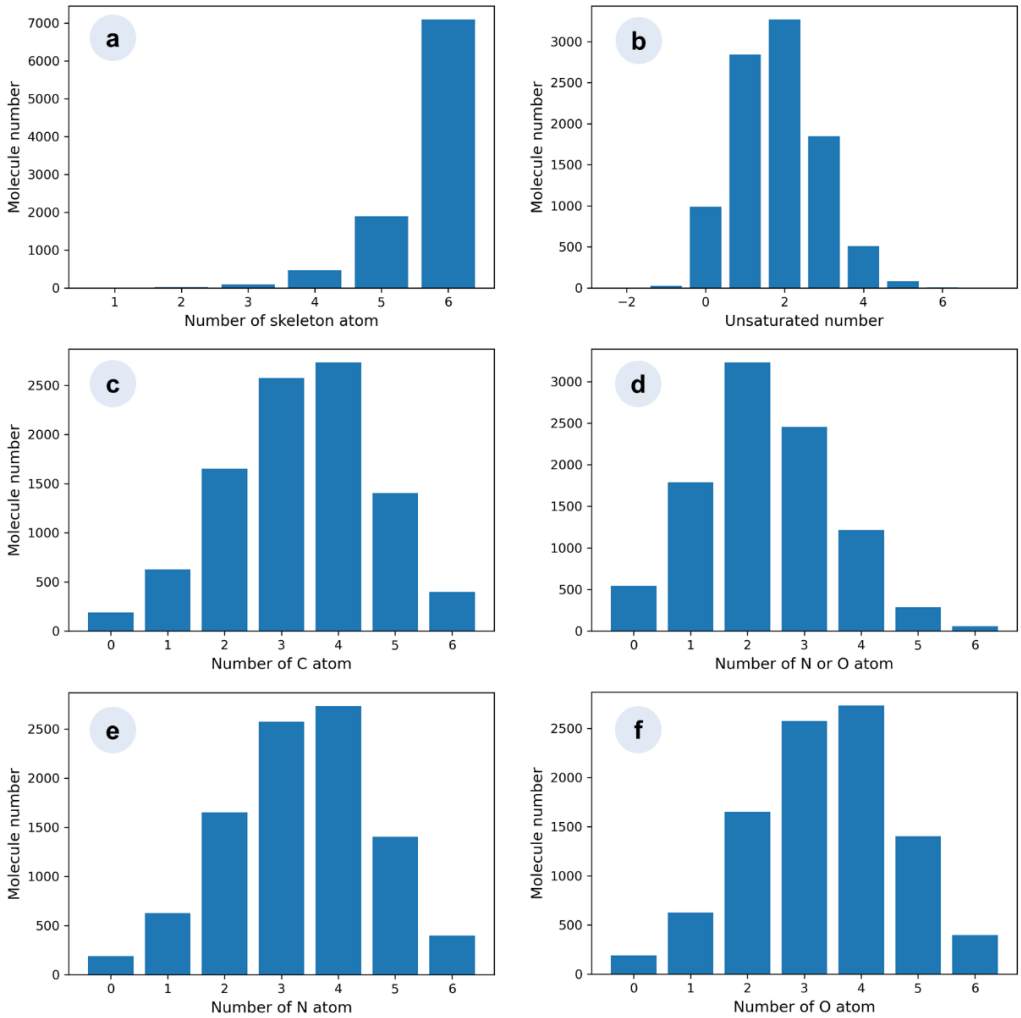

Supplementary Figure S1:The composition distribution of molecules and fragments adsorbed on Cu surfaces. Histograms of molecular compositions in the C–H–O–N dataset adsorbed on Cu surfaces, categorized by: (a) skeleton atoms (C, N, O); (b) degree of unsaturation number (calculated by: $\left(2 \times n(\mathrm{C}) + n(\mathrm{N}) - n(\mathrm{H})\right)/2 - 2$, $n(\mathrm{C})$,$n(\mathrm{N})$,$n(\mathrm{H})$ represent the number of respective elements); (c) carbon atoms; (d) nitrogen or oxygen atoms; (e) nitrogen atoms; (f) oxygen atoms.

Supplementary References

1. Schütt, K. T., Unke, O. T. & Gastegger, M. Equivariant message passing for the prediction of tensorial properties and molecular spectra. in *International Conference on Machine Learning* (2021).
2. Batatia, I., Kovacs, D. P., Simm, G., Ortner, C. & Csányi, G. MACE: Higher order equivariant message passing neural networks for fast and accurate force fields. *Adv. Neural Inf. Process. Syst.* **35**, 11423–11436 (2022).
3. Liu, Q.-Y., Chen, D., Shang, C. & Liu, Z.-P. An optimal Fe–C coordination ensemble for hydrocarbon chain growth: a full Fischer–Tropsch synthesis mechanism from machine learning. *Chem. Sci.* **14**, 9461–9475 (2023).
4. Batzner, S. *et al.* E(3)-equivariant graph neural networks for data-efficient and accurate interatomic potentials. *Nat. Commun.* **13**, 2453 (2022).
5. Musaelian, A. *et al.* Learning local equivariant representations for large-scale atomistic dynamics. *Nat. Commun.* **14**, 579 (2023).
6. Guo, Z.-X., Song, G.-L. & Liu, Z.-P. Artificial intelligence driven molecule adsorption prediction (AIMAP) applied to chirality recognition of amino acid adsorption on metals. *Chem. Sci.* **15**, 13369–13380 (2024).